ACS OMEGA

http://pubs.acs.org/journal/acsodf

Article

Cuproptosis-Mediated Patterns Characterized by Distinct Tumor Microenvironment and Predicted the Immunotherapy Response for Gastric Cancer

Xiang-Xu Wang,[‖] Shi-Zhou Deng,[‖] Li-Hong Wu,[‖] Qing-Qing Liu, Gaozan Zheng, Kunli Du, Qiong-Yi Dou, Jianyong Zheng,* and Hong-Mei Zhang*

Cite This: *ACS Omega* 2023, 8, 10851−10862

Read Online

ACCESS | Metrics & More | Article Recommendations | Supporting Information

ABSTRACT: Cuproptosis is a newly discovered programmed cell death process, and several cuproptosis-related genes have been reported to regulate cancer cell proliferation and progression. The association between cuproptosis and tumor microenvironment in gastric cancer (GC) remains unclear. This study aimed to explore multiomics characteristics of cuproptosis-related genes regulating tumor microenvironment and provide strategies for prognosis and prediction of immunotherapy response in GC patients. We collected 1401 GC patients from the TCGA and 5 GEO data sets and identified three different cuproptosis-mediated patterns, each of which shared a distinct tumor microenvironment and different overall survival. The GC patients with high cuproptosis levels were enriched in CD8+ T cells and had a better prognosis. Whereas, the low cuproptosis level patients were associated with inhibitory immune cell infiltration and had the worst prognosis. In addition, we constructed a 3-gene (AHCYL2, ANKRD6 and FDGFRB) cuproptosis-related prognosis signature (CuPS) via Lasso-Cox and multivariate Cox regression analysis. The GC patients in the low-CuPS subgroup had higher TMB levels, MSI-H fractions, and PD-L1 expression, which suggests a better immunotherapy response. Therefore, the CuPS might have the potential value for predicting prognosis and immunotherapy sensitivity in GC patients.

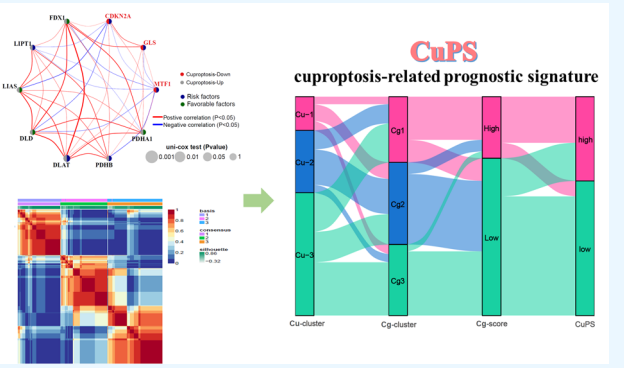

1. INTRODUCTION

Gastric cancer (GC) is the fifth most commonly diagnosed cancer and the fourth leading cause of cancer death globally.[1] Due to the insidious onset and high heterogeneity, most GC patients are diagnosed in the advanced stage, leading to poor prognosis.[2] With the continuous development of treatment methods, targeted therapy and immunotherapy, in addition to traditional therapy, have occupied a place in the treatment of gastric cancer, and targeted therapy site HER2 and immune checkpoint PD-LI have become important detection indicators for GC patients. Trastuzumab, a drug first applied to HER2-positive gastric cancer, is prone to drug resistance,[3,4] while the positive rate of checkpoint PD-LI patients used for immunotherapy is low, and immune checkpoint inhibitors (ICIs) are more differentiated due to individual differences in efficacy.[5] Therefore, it is essential to find new biomarkers of prognosis and efficacy prediction, for enriching the individualized treatment strategy of GC.

Copper ion is a necessary metal element in organisms (bacteria, animals, and humans), which can play an important role in the process of life activities as a cofactor of essential enzymes.[6] Under the normal physiological state, copper ions maintain a low concentration and dynamic balance in the organism, whereas the abnormal accumulation of copper ions can cause copper toxicity, and then induce cell death.[7,8] Studies have shown that mutations in human genes can lead to the imbalance of copper homeostasis and induce a variety of diseases, and its metabolic abnormalities can cause anemia, CCS syndrome, and congenital glycosylation disorders, as well as cancers.[9−13] It has been reported that copper imbalance promotes metastasis amplification through the OX-ATP7A-LOx pathway.[14] In addition, several studies have found that copper ion carriers and their chelating agents are expected to be potential drug molecules for tumor therapy.[15−17] However, the molecular specific mechanism of the copper-mediated cell death remains unclarified.

Cuproptosis or copper death is the latest proposed programmed cell death.[18] The metabolites in the tricarboxylic

Received: November 1, 2022
Accepted: February 28, 2023
Published: March 16, 2023

ACS Publications

© 2023 The Authors. Published by American Chemical Society

acid (TCA) are involved in regulating cuproptosis during mitochondrial respiration. The proposed concept of copper death deepens the understanding of the regulation of copper metabolism in tumors. Therefore, the exploration of the molecular mechanism of copper toxicity leading to cell death is helpful for the further understanding of human copper imbalance diseases and the development of treatment strategies.

In this paper, we integrated multiomics and clinical information on 1401 gastric cancer patients from 5 GEO gastric cancer data sets and the TCGA-STAD data set. On the basis of the transcriptome characteristics of 10 cuproptosis-related genes (Cu-RGs), we identified 3 cuproptosis-mediated patterns (Cu-clusters) characterized by different immune microenvironments, and presented different prognoses. We further established a cuproptosis scoring system (Cg-score) and a cuproptosis-related prognosis signature (CuPS) to estimate the cuproptosis-mediated patterns in individual patients. The CuPS was significantly correlated with TMB, MS status PD-L1 expression, the immune microenvironment, and drug sensitivity, which might might make it a potential biomarker for prognosis and immunotherapy response prediction in gastric cancer.

2. MATERIALS AND METHODS

2.1. Data Acquisition. A total of 1401 GC samples with expression (RNA-seq) and corresponding clinical data were collected from TCGA-STAD, GSE15459, GSE34942, GSE57303, GSE62254, and GSE84437 data sets. Samples with missing clinical data were excluded from subsequent studies. The FPKM format expression data of TCGA-STAD was converted into TPM format[19] and further merged with other 5 GEO cohorts. The batch effects were removed using the "ComBat" method by the R package "SVA".[3]

The copy number variation (CNV) data of TCGA-STAD were downloaded from the UCSC Web site https://xena.ucsc.edu/, while the single nucleotide variants data were downloaded from the TCGA database https://portal.gdc.cancer.gov/. The data of 5 GEO cohorts were downloaded from the GEO database https://www.ncbi.nlm.nih.gov/geo/.

2.2. Identification of Cuproptosis-Mediated Patterns by NMF Unsupervised Clustering Algorithm. The 10 Cu-RGs was collected from a *Science* paper which were identified by whole genome CRIPSR/Cas9 positive selection screen.[18] The 10 Cu-RGs included seven cuproptosis positive regulators (FDX1, LIPT1, LIAS, DLD, DLAT, PDHA1, PDHB) and three negative regulators (MITF1, GLS and CDKN2A).[18] We performed unsupervised clustering by non-negative matrix factorization (NMF) to identify distinct Cuproptosis-mediated patterns.[20] According to dispersion, silhouette coefficients, and cophenetics, we selected the optimal number of clusters. To ensure the stability of the consensus clusters, we performed the brunet algorithm in the "NMF" package and repeated it 1000 times.[21]

2.3. Gene Set Variation Analysis (GSVA) and Functional Annotation. The GSVA analysis[22] performed by the "GSVA" package was used to investigate the difference of biological process among different cuproptosis subtypes (Cu-clusters). The "hallmark" gene sets were downloaded from the MSigDB database.[23] The inclusion criteria for statistically significant pathways were adjusted P value <0.05. Adjusted P value <0.05 was considered statistically significant. Functional annotation for the selected genes were conducted by the "clusterProfiler" package,[24] and an FDR < 0.05 was selected as the cutoff value.

2.4. Estimation of Immune Cell Infiltration. The CIBERSORT algorithm and "MCPcounter" packages were conducted to quantify the fraction of infiltrating immune cells in each GC sample. A total of 22 immune cells evaluated by CIBERSORT were performed to map the immune invasion of the tumor microenvironment.[25] The "MCPcounter" package was applied to estimate the fraction of fibroblasts, endothelial cells, and eight different immune cells.[26]

2.5. Identification of Cu-Clusters Related and Differently Expressed Genes (Cu-DEGs). A total of 470 Cu-DEGs were identified by the "limma" package among three GC Cu-clusters, with the adjusted P value <0.05 and |logFC > 0.1| as the significance criteria.[27] Eighteen prognosis-significant genes were further identified in GEO-meta, GSE84337, and TCGA-STAD cohorts (P < 0.05). The expression of 18 prognosis-significant Cu-DEGs among three GC Cu-clusters was illustrated by heatmap.

2.6. Identification of Cuproptosis-Related Gene Subtypes and Construction of the Cuproptosis Gene Signature (Cg-Score). We identified three distinct cuproptosis-related gene subtypes based on the expression of 18 Cu-DEGs via the "NMF" algorithm. And we constructed a cuproptosis gene signature (termed as Cg-score) to evaluate the cuproptosis mediate patterns of individual GC samples. On the basis of the identified 18 prognosis-significant Cu-DEGs, we constructed the Cg-score via principal component analysis (PCA) similar to previous studies.[28,29] The formula was as follows: Cg-score = $\sum(PC1_i + PC2_i)$, and the "i" presented the expression of 18 prognosis-significant Cu-DEGs. This method concentrated the Cg-score on the set of genes with good correlation (or anticorrelated), and reduced the contributions of genes from other sets.

2.7. Construction of the Cuproptosis-Related Prognostic Signature (CuPS). In the GEO-training cohort, we further explored the prognostic hub genes with LASSO-Cox and multivariate Cox regression, and finally constructed a cuproptosis-related prognostic signature (termed as CuPS). Eight genes were selected by LASSO-Cox regression via the "glmnet" packages, and three hub genes (AHCYL2, ANKRD6, and FDGFRB) were finally screened by multivariate COX analysis with "both step" function.[30] The formula of CuPS was defined as follows: CuPS = $-0.205*AHCYL2_{exp} + 0.231*ANKRD6_{exp} + 0.238*FDGFRB_{exp}$, where "exp" signifies the expression. The packages the "survivalROC" and "survminer" were utilized to compute the receiver operating characteristic curve (ROC) and Kaplan−Meier (K−M) survival curve. The optimal cutoff value of CuPS (1.1) was identified via the "surv_cutpoint" function in the training cohort, and the patients were classified into the high- and low-CuPS subgroups in the training, testing, GSE84337, and TCGA-STAD cohorts by the same cutoff value.

2.8. Survival Meta-Analysis of AHCYL2, ANKRD6, and FDGFRB. To explore the prognosis value of 3 selected hub genes (AHCYL2, ANKRD6, and FDGFRB), we performed the survival meta-analysis in six independent gastric cancer cohorts via "meta" packages.[31] Considering the heterogeneity among different cohorts, we used a random-effects model to calculate the pooled prognosis effect values of each gene.[32]

2.9. qRT-PCR and Immunohistochemistry of AHCYL2, ANKRD6, and FDGFRB. Quantitative real-time PCR (qRT-PCR) was performed to validate the expression levels of

https://doi.org/10.1021/acsomega.2c07052
ACS Omega 2023, 8, 10851−10862

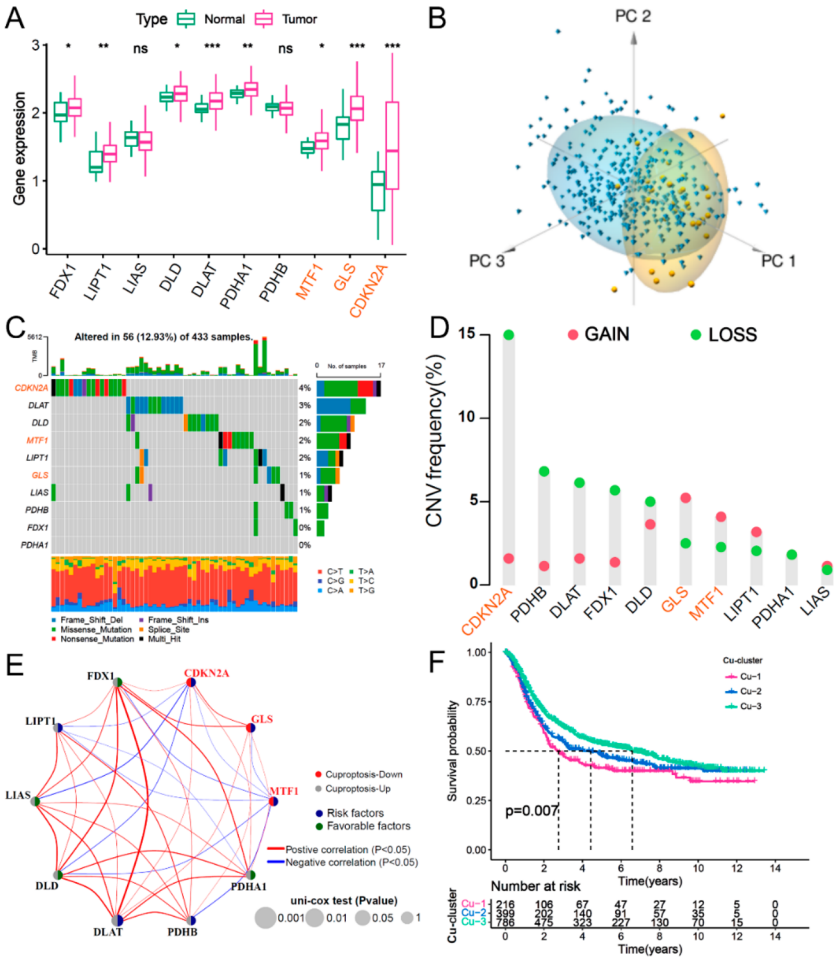

Figure 1. Multiomics characteristics of 10 Cu-RGs in gastric cancer and identification of cuproptosis subtypes. (A) Comparison of Cu-RGs expression between gastric cancer and normal tissues. (B) Three-dimensional PCA analysis of Cu-RGs in gastric cancer and normal tissues, blue and yellow scatters represent cancer and normal tissues, respectively. (C) An overview of 10 Cu-RGs mutation characteristics in the TCGA-STAD cohort. (D) CNV frequency of 10 Cu-RGs in the TCGA-STAD cohort. (E) Pairwise correlation of Cu-RGs gene expression, and univariate Cox analysis for each Cu-RG. The thickness of the lines represent the correlation coefficient. The size of the points represent the *P* value in univariate Cox analysis. (F) Survival analysis for patients in multiple databases, patients were classified by Cu-cluster. Abbreviation: PC, principal component; ns, no significant difference; *, $P < 0.05$; **, $P < 0.01$; ***, $P < 0.001$.

AHCYL2, ANKRD6, and FDGFRB in normal (GES1) and GC (AGS and N87) cell lines. The qRT-PCR was applied by C1000 system (Bio-Red, Hercules, CA) and SYBR Green Mix (TaKaRa RR820A, Japan). The sequences of primers were as follows: AHCYL2-F: TTCAACAAACGTCCCACCAAA, AHCYL2-R:CCTGGGCGATG TCTCATCA; ANKRD6-F: GTCGCTGCACTTTCAGAGC, ANKRD6-R:CCATGCT TGGTAACCGCTAC; PDGFRB-F: AGCACCTTCGT-TCTGACCTG, PDGFRB-R: TATTCTCCCGTGTCT-AGCCCA. The immunohistochemistry information on AHCYL2, ANKRD6, and FDGFRB were collected from the "The Human Protein Atlas" database, https://www.proteinatlas.org/.

2.10. Prediction of CuPS in Drug Sensitivity and Immunotherapy Response. We collected pharmacogenomic data from the Genomics of Drug Sensitivity in Cancer (GDSC) database and calculated the IC50 of different drugs by the "pRRophetic" package.[33] The correlation (Spearman) between IC50 values of drugs and the CuPS was calculated, with criteria of the significant correlations were |Corl > 0.2 and adjusted $P < 0.05$. The immunotherapy data set was collected from the IMvigor210 cohort (urinary tract transitional cell carcinoma), and was treated with PD-L1 inhibitor (Atezolizumab).[34,35] The CR (complete response) and PR (partial response) were considered as immunotherapy responses, while SD (stable disease) and PD (progressive disease) were considered as no-response.

2.11. Statistical Analysis. The Perl 5 (version 30) and R software (version 4.0.2) were applied to complete Bioinformatics and statistical analysis in this study. The "maftools" package was used to draw the waterfall plot to present the mutation landscape in GC samples, and the "Rcircos" package was conducted to present the copy number variation. The differences between two groups were compared by Wilcoxon rank-sum test, while three groups were compared by the Kruskal–Wallis tests. The significance criterion was $P < 0.05$, and the false discovery rate (FDR) was used for multiple hypothesis tests. All tests were bilateral.

3. RESULTS

3.1. Multiomics Characterization of Cuproptosis-Related Genes in Gastric Cancer and Identification of Cuproptosis-Mediated Patterns. The flowchart is shown in Figure S1 of the Supporting Information. In this study, a total

https://doi.org/10.1021/acsomega.2c07052
ACS Omega 2023, 8, 10851−10862

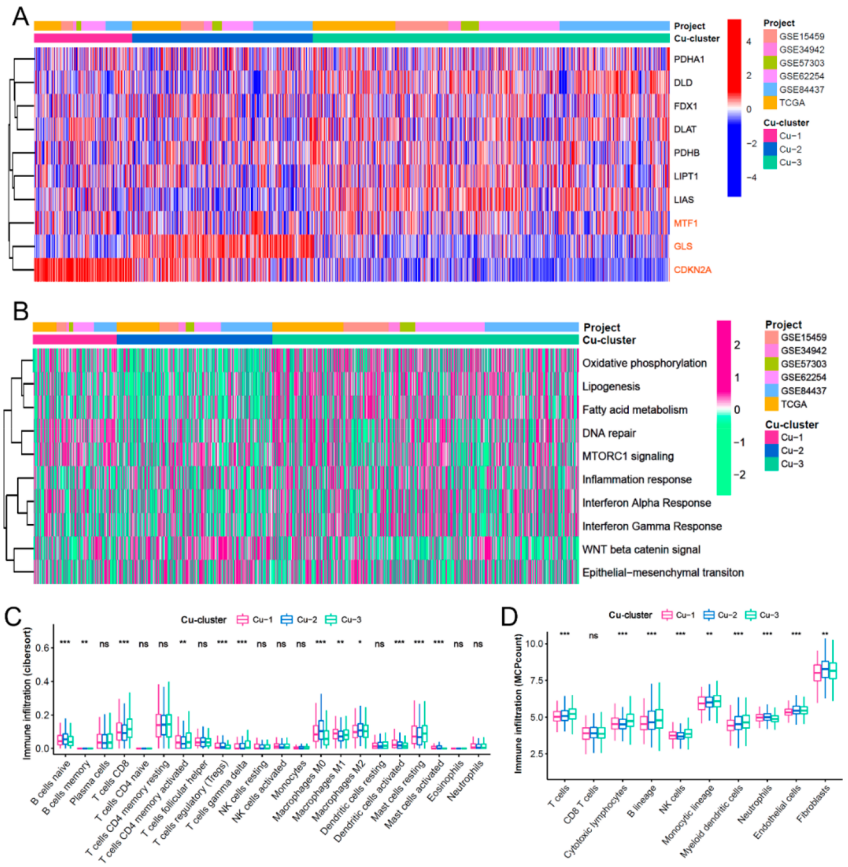

Figure 2. Differential gene enrichment and immune cell infiltration analysis among three distinct Cu-clusters. (A) Normalized expression heatmap of 10 Cu-RGs among three Cu-clusters in 6 different GC databases. (B) GSVA score heatmap of cancer-related pathways among three Cu-clusters. (C, D) The fraction of TME cells infiltration among three distinct Cu-clusters based on CIBERSORT (C) and MCPcount (D) algorithms.

of 1401 gastric cancer patients with complete transcriptome and survival information were collected from 5 GEO gastric cancer data sets and the TCGA-STAD data set. The 10 cuproptosis-related genes (Cu-RGs) were obtained from the published literature.[18] First, we compared the expression of 10 Cu-RGs between GC and in normal tissues. The result has shown that the 3 downregulated Cu-RGs (MITF1, GLS, and CDKN2A) were significantly more highly expressed in tumor tissues than in normal tissues (Figure 1A). And the expression of 10 Cu-RGs could distinguish tumors from normal tissues in the 3D-PCA plot (Figure 1B). The mutation landscape showed that 56 of 433 (12.93%) GC patients experienced mutation of the 10 Cu-RGs (Figure 1C). The investigation of copy number alteration (CNA) frequency showed that most of the Cu-RGs were prevalently focused on the deletion in copy number. CDKN2A led the highest frequency of CNA deletion, while GLS had the highest frequency of CNA amplification (Figure 1D). We further performed the pairwise correlation analysis of Cu-RGs gene expression, and univariate Cox analysis for each Cu-RG (Figure 1E). The results showed that the negative cuproptosis genes (CDKN2A, MTF1, and GLS) in GC patients were significantly negative corrected with the positive cuproptosis genes and were the risk factors for overall survival (OS).

The non-negative matrix factorization (NMF) algorithm was applied to classify 1401 GC patients into three distinct cuproptosis-mediated patterns, termed as Cu-cluster 1 (n = 216), Cu-cluster 2 (n = 399), and Cu-cluster 3 (n = 786) based on the expression of 10 Cu-RGs (Figure S2A-I). K−M survival analysis showed that Cu-3 had the best OS, followed by Cu-cluster 2 and Cu-cluster 1 (P = 0.007, Figure 1F).

3.2. Differential Gene Enrichment Analysis of Cuproptosis-Mediated Patterns and Immune Cell Infiltration. To discover the underlying biological mechanisms behind the differences in survival between the three Cu-clusters, we estimated the gene sets enrichment analysis score (GSEA) and immune cell infiltration. The results showed that CDKN2A was highly expressed in Cu-cluster 1, GLS was highly expressed in Cu-cluster 2, and both CDKN2A and GLS were low expressed in Cu-cluster 3 (Figure 2A). Therefore, we speculated that patients with low expression of CDKN2A and GLS had a better prognosis than patients with high expression. The result of GSEA showed that the Cu-cluster 1 was enriched in mTORC1 signaling, DNA repair, and G2M checkpoint pathways. While Cu-cluster 3 was noted in metabolism pathways, such as lipogenesis, oxidative phosphorylation, peroxisome, lipogenesis, and fatty acid metabolism. The Cu-cluster 2 was enriched in WNT beta catenin signal, glycolysis, and epithelial-mesenchymal transition (Figure 2B). We further analyzed the immune cell infiltration by both CIBERSORT (Figure 2C) and MCPcounter algorithms (Figure 2D). The GC patients in Cu-cluster 3 were significantly enriched in lymphocyte infiltration, such as T cells and NK cells. The Cu-cluster 2 was associated with inhibitory immune cell infiltration, such as M2 macrophage, Tregs, endothelial, and fibroblasts. And Cu-cluster 1 was associated with the immune-desert with low immune cell infiltration.

https://doi.org/10.1021/acsomega.2c07052
ACS Omega 2023, 8, 10851−10862

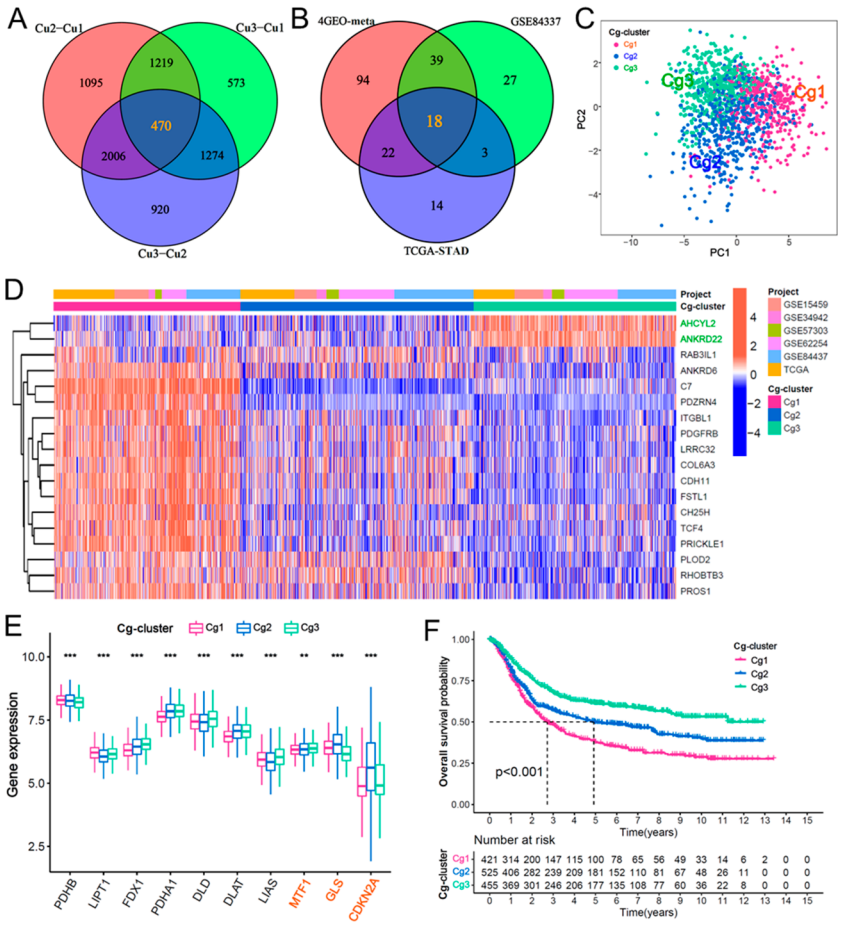

Figure 3. Identification and survival analysis of Cu-RG subtypes. (A) Venn diagram for the intersection of cuproptosis related differentially expressed genes (Cu-DEGs) among Cu-1, Cu-2, and Cu-3 pairwise comparison. (B) The intersection of Cu-DEGs in 4 GEO data sets, GSE84437 and TCGA-STAD. (C) PCA clustering using 18 Cu-DEGs in all the data sets, the dots in purple, blue, and green represented Cg-1, Cg-2, and Cg-3 clusters, respectively. (D) Expression heatmap and comparison of 18 Cu-DEGs in different Cg-clusters. (E) Expression comparison of 18 Cu-DEGs among three different Cg-clusters by one-way ANOVA analysis. (F) Overall survival (OS) analysis of among three distinct Cg-clusters.

3.3. Identification and Survival Analysis of Cuproptosis-Related Genes Subtypes. To explore the copper death related gene subtypes, we identified 470 differentially expressed genes (DEGs) among three subtypes (Figure 3A). In addition, 18 prognostic significant DEGs were finally identified among GEO-meta, GSE84337, and TCGA-STAD cohorts (all $P < 0.05$, Figure 3B). On the basis of the expression of 18 prognostic significant DEGs, we further identified three different clusters (termed as Cg-cluster 1, Cg-cluster 2, and Cg-cluster 3) via "NMF" algorithm (Figure S3A−I). Three Cg-clusters could be clearly identified by PCA analysis (Figure 3C). In Cg-cluster 3, AHCYL2 and ANKRD22 were highly expressed, and the other genes all showed low expression, while the Cg-cluster 1 was the opposite (Figure 3D). The patients in Cg-cluster 3 were overexpressed in most cuproptosis positive genes and significantly down-expressed in GLS and CDKN2A, which suggests a high cuproptosis level (Figure 3E). The K−M survival analysis also showed that Cg3 had the best OS, followed by Cg2 and Cg1 ($P < 0.001$, Figure 3F).

3.4. Cg-Score Was Associated with Tumor Mutation Burden (TMB) and Microsatellite Instability (MS) Status. We further constructed a cuproptosis scoring system (Cg-score) by PCA analysis to estimate the cuproptosis-mediated patterns in individual patients, and analyzed its correlation between Cg-clusters and Cu-clusters. The results showed that Cg1 had a higher Cg-score than Cg2 and Cg3 (Figure 4A), and the Cu-3 had the highest Cg-score, followed by Cu-2 and Cu-1 (Figure 4B). The K−M survival analysis showed that low Cg-score had a better OS ($P < 0.001$, Figure 4C). Next, we compared the tumor mutations burden (TMB) between two Cg-Score subgroups, and found that the TMB was higher in the low CG-Score group (Figure 4D). The mutation landscape of the TGCA-STAD cohort showed that 81 of 104 samples with high CG-Score were detected mutation. And 220 of the 237 (92.44%) in the low CG-Score samples had mutations (Figure 4E). Through comprehensive analysis of mutations in the three Cg-clusters, it was found that the Cg-score was significantly negatively correlated with TMB (cor = −0.38, $P < 0.001$, Figure 4F). And the K−M survival analysis showed that H-TMB had the best OS ($P < 0.001$, Figure 4G). However, the Cg-score in different MSI statuses did not show a significant difference ($P > 0.05$, Figure 4H).

3.5. Construction and Validation of Cuproptosis-Related Prognostic Signature (CuPS). To further understand the relationship between cuproptosis and the prognosis of GC patients, the Lasso-Cox and multivariate Cox were applied to screen the cuproptosis-related and prognostic significant hub genes. A total of 8 prognostic DEGs were selected through Lasso-Cox (Figure S4A,B), and 3 prognostic

https://doi.org/10.1021/acsomega.2c07052
ACS Omega 2023, 8, 10851−10862

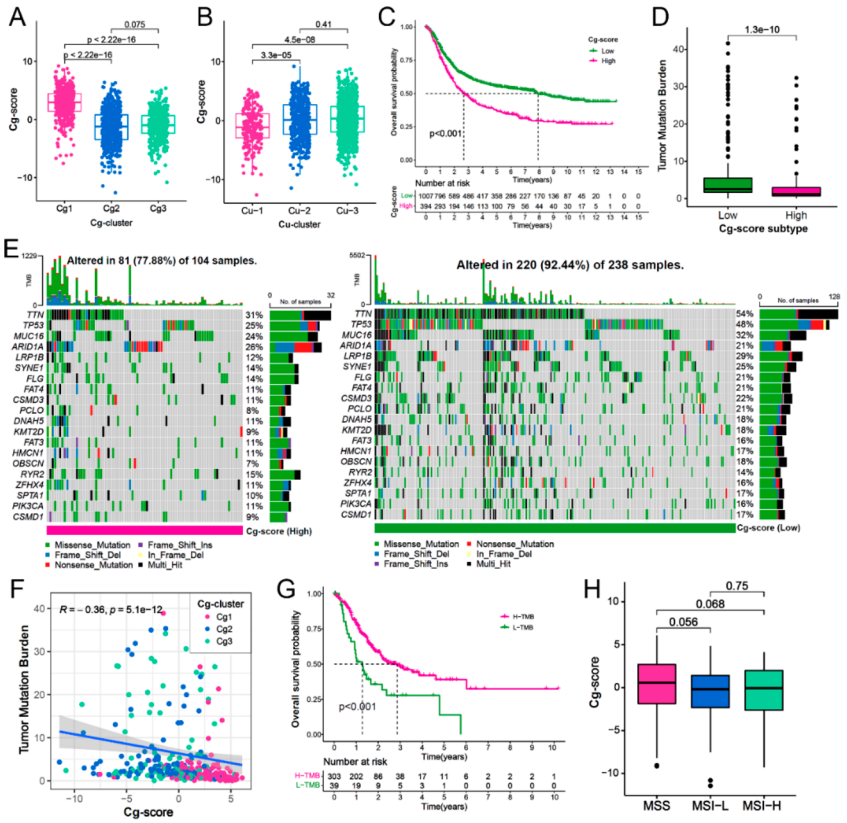

Figure 4. Cg-score was associated with tumor mutation burden (TMB) and microsatellite instability (MS) status. (A, B) Comparison of Cg-score among different Cg subtypes (A) and Cu subtypes (B). (C) Kaplan−Meier analysis of OS between Cg-high and Cg-low subtypes. (D) TMB of Cg-high and Cg-low patients. (E) Somatic mutation atlas of top 20 genes between Cg-high (left) and Cg-low (right) subtypes. (F) Relationship between Cg-score and TMB calculated by Pearson correlation analysis. (G) Survival analysis of TMB-high and TMB-low patients. (H) Comparison of Cg-score among patients with different MSS, MSI-L, and MSI-H status.

hub DEGs were finally identified via multivariate Cox. The hazard ratio and *P* values of these selected genes were shown in the forest diagram of univariate Cox (Figure S4C,D). The hub DEGs AHCYL2 was a favorable factor for GC prognostic, while other hub DEGs (ANKRD6 and PDGFRB) were risk factors. To further confirm the prognostic value of 3 hub genes (AHCYL2, ANKRD6, and PDGFRB) in GC, we explored the K−M survival analysis in the training cohort, testing, GSE84337, and TCGA independent cohort, respectively (Figure S5A−L). As expected, the prognostic value of AHCYL2, ANKRD6, and PDGFRB were further confirmed in 6 independent GC cohorts via survival meta-analysis (Figure S6A−C). In addition, we performed RT-qPCR to validate the expression levels of the 3 hub genes between normal (GES1) and GC (AGS and N87) cell lines. The result showed that the AHCYL2 was significantly less expressed in AGS and N87 GC cell lines, while the ANKRD6 and PDGFRB were significantly highly expressed in AGS and N87 GC cell lines (Figure S7A,C,E). We explored the protein expression of 3 hub genes in the "The Human Protein Atlas" database. The immunohistochemistry showed that the AHCYL2 was negatively expressed in all 10 CG patients (Figure S7B), the ANKRD6 was positively expressed in 9 of 10 GC patients (Figure S7D), and the PDGFRB was positively expressed 3 of 10 GC patients (Figure S7F).

We further constructed a cuproptosis related prognostic signature termed as CuPS via multivariate Cox. The patients with increasing CuPS had a high fraction of death and shorten survival time in training, testing, GSE84337 and TCGA-STAD cohort (Figure 5A-D, Figure S8A−D). In addition, the patients in training, testing, GSE84337 and TCGA-STAD cohorts with low CuPS led a significantly longer OS benefit (Figure 5E−G). The receiver operating characteristic (ROC) curves were utilized to estimate the prediction performance of CuPS. The AUC for 1-, 2-, and 3- year OS was 0.655, 0.625, 0.652 in the training cohort, 0.618, 0.591, 0.645 in the testing cohort, 0.573, 0.575, 0.577 in the GSE84337 cohort and 0.600, 0.604, 0.601 in the TCGA-STAD cohort, respectively (Figure 5I−L).

3.6. Analysis of the Related Features of Cu-Related Gene Prognostic Signature (CuPS). Consistent with the above findings, the alluvial diagram illustrated the analysis workflow of Cu-cluster, Cg-cluster, Cg-score, and CuPS (Figure 5A). And the consequences showed that Cu-cluster 3 associated with Cg-cluster 3 exhibited a lower Cg-score and lower CuPS (Figure 6A). The K−M survival analysis showed that patients in the "L−Cg+L−Cu" group had the best OS, while the "H−Cg+H−Cu" group had the worst OS ($P < 0.001$, Figure 6B). Compared with Cu-1 and Cu-2, the patients in the Cu-3 group had the lowest CuPS (Figures 6 B). And patients in the Cg-1group had the highest CuPS, followed by Cu-2 and Cu-1 (Figure 6 C). In addition, the tumor burden mutation (TMB) was significantly higher in the low-CuPS group than high-CuPS group (Figure 4E), and the CuPS was negatively correlated with TMB ($R = -0.45$, Figure 4F). The waterfall diagrams of the top 20 frequent mutation genes were exhibited in Figure 6G. The patients with low CuPS had significantly high mutation frequently in TTN, MUC16, and ARID1A.

https://doi.org/10.1021/acsomega.2c07052
ACS Omega 2023, 8, 10851−10862

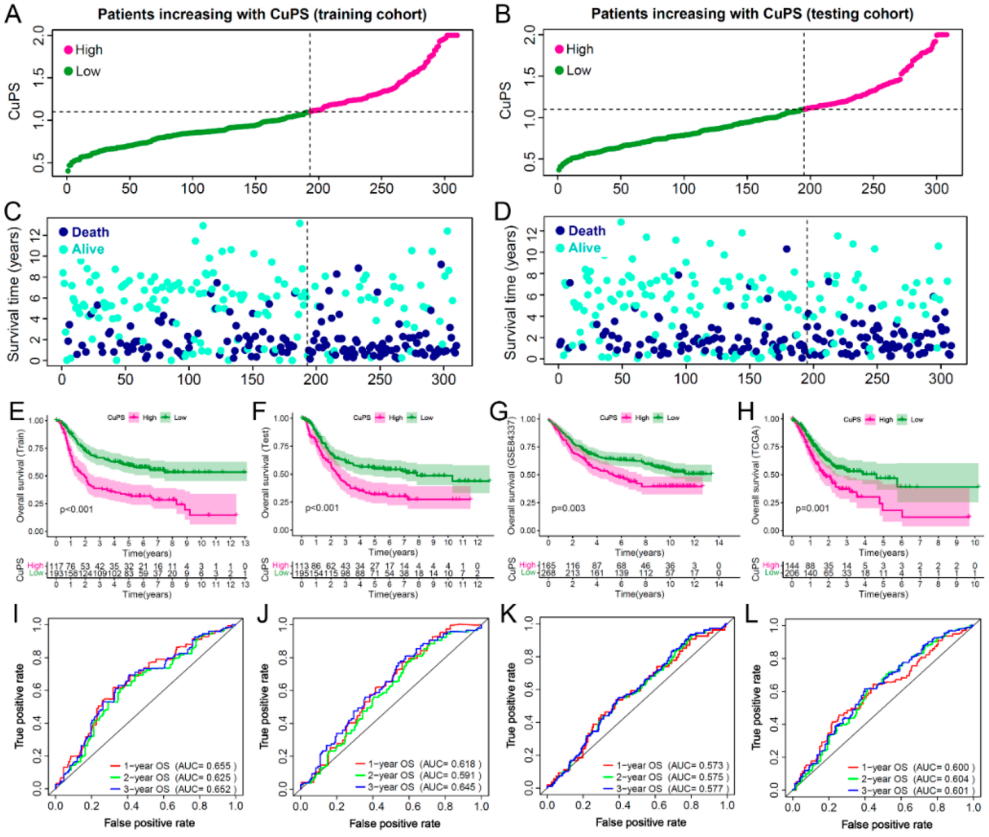

Figure 5. Construction and validation of cuproptosis-related prognostic signature (CuPS). (A, B) patients with increasing CuPS in training (A) and testing cohorts (B). (C, D) Overall survival time and living status of patients with increasing CuPS in training (C) and testing cohorts (D) cohort. The numbers of *x*-axis were presented the rank of patient ordered by the CuPS. (E−H) K−M analysis of OS for patients between high-CuPS and low-CuPS subgroups in training (E), testing (F), GSE84437 (G), and TCGA-STAD (H) cohorts, respectively. (I−L) Time-ROC curve for predicting 1-, 2-, and 3- year OS in training (I), testing (J), GSE84437 (K), and TCGA-STAD (L) cohorts, respectively.

3.7. Association of CuPS between Drug Sensitivity and Immunotherapy Response. In order to clarify the value of CuPS in GC treatment, we explored the drug sensitivity analysis and immunotherapy response prediction. We identified 15 anticancer drugs in the GDSC database were significantly associated with CuPS by Spearman correlation analysis (Figure 7A). The IC-50 of Ponatinib (AP24534), Rucaparib (AG-014699), and Motesanib (AMG-706) were notably negative correlated with CuPS, while the A.443654 (Akt1, 2, and 3 inhibitors) and AKT.inhibitor.VIII were positively correlated with CuPS.

The immune microenvironment has an important impact on tumor immunotherapy, we found that the CuPS was significantly positively correlated with endothelial cells and fibroblasts (Figure 7B). And patients in the low-CuPS subgroup had higher MSI-H fraction than the high-CuPS subgroup (27% vs 3%, Figure 7C), which indicated better immunotherapy response. In addition, the CuPS in MSS and MSI-L subgroups was significantly higher than the MSI-H subgroup (Figure 7D), and the patients in the low-CuPS subgroup showed higher PD-L1 expression (Figure 7E). We further validated the predictive value of CuPS for immunotherapy response in an immunotherapy cohort (IMvigor-210). The fraction of complete response (CR) and partial response (PR) in low-CuPS subgroup were higher than the high-CuPS subgroup (Figure 7F), and patients with CR/PR had a lower CuPS (Figure 7G). The K−M survival analysis also confirmed that the patients under immunotherapy in low-CuPS subgroup had a better OS benefit (P = 0.009, Figure 7H). In summary, these findings suggest that CuPS may provide more selective strategies for drug selection and immunotherapy response prediction.

4. DISCUSSION

The content of copper in the body is relatively stable, too high or too low can cause cell dysfunction, and lead to cell death. The intake, excretion, and metabolism of copper ions are regulated by multiple factors and maintain dynamic balance. When the copper homeostasis broken, it will lead to diseases such as Menkes disease, Wilson's disease, Alzheimer's disease, and even cancer. Increasing studies have highlighted the importance of copper metabolism in tumor biological processes. Compared with normal cells, some cancers have a higher demand for copper and express a large number of lipid acylated mitochondrial proteins and show a high intensity of respiration.[36] Wang et al. found that blocking Cu_2^+transport can cause oxidative stress in cells, reduce the level of ATP in cells, and activate AMP protein kinase, resulting in reduced fat production and inhibition of tumor cell proliferation.[37] Studies confirm that copper and hypoxia-inducible factor-1 α(HIF1-α) level was closely related. The HIF1-α can stimulate angiogenesis, and neovascularization can also induce the production of vascular endothelial growth factor, which then leads to rapid angiogenesis of the tumor.[38,39]

Cuproptosis is a new kind of programmed cell death (PCD) that has recently attracted widespread attention. The

https://doi.org/10.1021/acsomega.2c07052
ACS Omega 2023, 8, 10851−10862

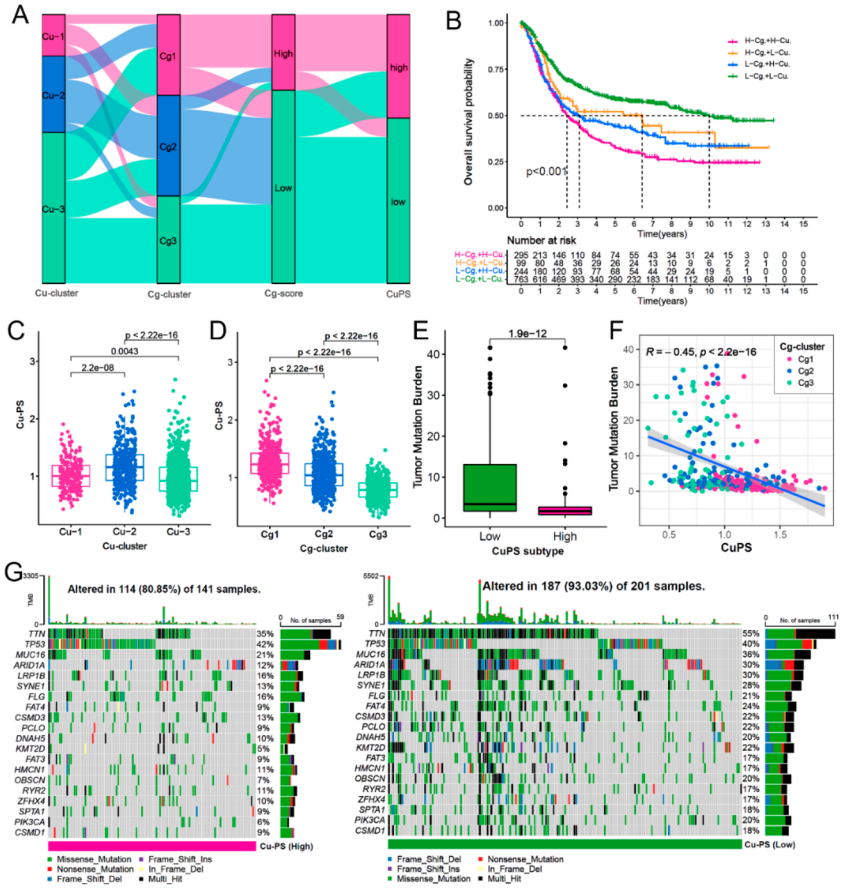

Figure 6. Correlation analysis of CuPS between clinical features and tumor mutation burden. (A) The alluvial diagram showed the association among different Cu-cluster, Cg-cluster, Cg-score, and Cu-PS. (B) K−M analysis of GC patients cross-classified by Cg-score and CuPS. (C, D) Comparison of CuPS among different Cu subtypes (C) and Cg subtypes (D). (E) Comparison of TMB between high- and low-CuPS subtypes. (F) Correlation scatter plot between CuPS and TMB, the dots in red, blue and green presented Cg1, Cg1, and Cg3 clusters, respectively. (G) Somatic mutation atlas of patients between high- and low-CuPS subtypes in TCGA-STAD cohort. Abbreviation: H-Cg, Cg-score high; L-Cg, Cg-score low; H-Cu, Cu-score high; L-Cu, Cu-score low.

association between cuproptosis and TCA suggests a correlation between this programmed death mechanism and cancer metabolism. In general, cells dependent on aerobic respiration are more sensitive to copper death than cells dependent on glycolysis. This characteristic distinguishes the cuproptosis from ferroptosis. Mitochondrial stress, especially the accumulation of lipoacylated mitochondrial enzymes and the loss of Fe−S cluster proteins, can lead to cuproptosis. Cuproptosis is associated with multiple cellular processes, including mitochondrial respiration, autophagy, antioxidant defense, and redox signaling, which are closely related to the tumor immune microenvironment. In gastric cancer, it is still not clear how copper death affects the immune microenvironment. The relationship between cuproptosis and the immune microenvironment is helpful to screen potential beneficiaries of ICIs in gastric cancer and improve the effect of immunotherapy.

In this study, we explored multiomics analysis of 10 cuproptosis-related genes (Cu-RGs) in 1401 gastric cancer patients collected from 5 GEO gastric cancer data sets and the TCGA-STAD cohort. The expression, somatic mutation, and copy number variation landscapes suggest a broad association between Cu-RGs and gastric cancer. We further identified three cuproptosis patterns that shared distinct tumor microenvironment, and had different overall survival prognoses. Our results showed that the GC patients in Cu-3 cluster were enriched in oxidative phosphorylation, lipogenesis, and fatty acid metabolism pathways. Oxidative phosphorylation and fatty acid metabolism depend on mitochondrial function and increase mitochondrial oxidative stress,[40] suggesting that the patients in the Cu-3 cluster may be more sensitive to cuproptosis. In addition, the Cu-3 patients had significant better overall survival, which suggests that higher sensitivity to cuproptosis is associated with better prognosis in gastric cancer. Given the important roles of INF-α, INF-γ, and WNT (β-catenin) pathways in modulating immune responses and infiltrating immune cells in cancers,[41−44] the differences in the levels of these pathways among the three cuproptosis patterns suggest a closely association between cuproptosis levels and tumor immune microenvironment. Two different algorithms of infiltrating immune cells assessment confirmed these findings that the Cu-3 patients had higher levels of immune effector cell (CD8+ T cell) infiltration, whereas Cu-1 was associated with inhibitory immune cell infiltration, and had the worst prognosis.

Furthermore, we identified three hub cuproptosis-related prognostic significant genes (AHCYL2, ANKRD6, and PDGFRB) by Lasso-Cox and multivariate COX analysis, and further established a cuproptosis-related prognostic signature (CuPS). Among the 3 hub genes, AHCYL2 is closely

https://doi.org/10.1021/acsomega.2c07052
ACS Omega 2023, 8, 10851−10862

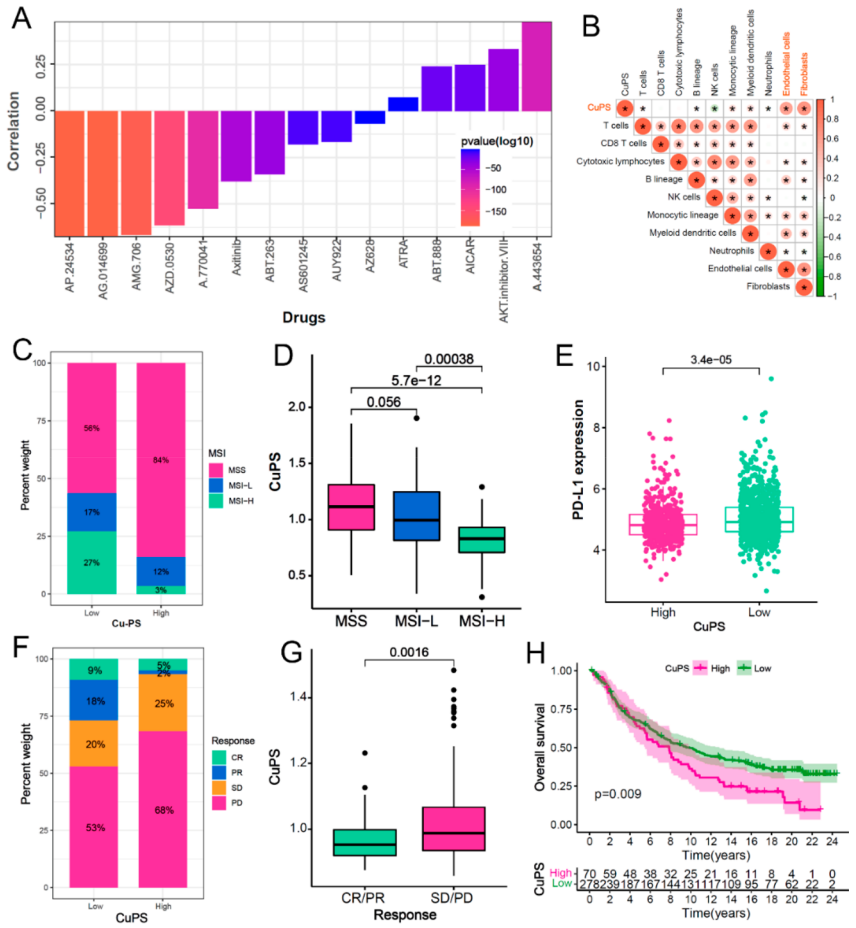

Figure 7. Association of CuPS between drug sensitivity and immunotherapy response. (A) Correlation between CuPS and IC50 of drugs in GSDC database. (B) Correlation between CuPS and immune cells infiltration (MCPcount). The size of the dot indicated the strength of the correlation, and the red dot presented positive correlation, and the green dot presented negative correlation. (C) The proportion of patients in different microsatellite (MS) status between high- and low-CuPS subgroup. (D) Comparison of CuPS among different MS status. (E) Comparison of PD-L1 expression between high- and low-CuPS subgroup. (F) The proportion of patients in different immunotherapy response (CR, PR, SD, and PD) between high- and low-CuPS subgroup in IMvigor-210 cohort. (G) Comparison of CuPS between response (CR/PR) and nonresponse (SD/PD) patients in IMvigor-210 cohort. (H) K−M analysis of OS between high- and low-CuPS patients in IMvigor-210 cohort.

associated with copper transport and cuproptosis. This gene may be involved in the conversion of S-homocysteine to L-homocysteine, one carbon metabolism and transport of glucose, metal ions, bile salts, and amine compounds. ANKRD6 is a key regulatory molecule of the WNT/β-catenin pathway, which was involved in NAD binding and adenosyl homocysteinase activity.[45,46] ANKRD6 (Ankyrin repeat domain 6) ANKRD6 promotes β-catenin degradation and phosphorylation, thereby inhibiting β-catenin/Tcf signaling.[47] PDGFRB plays a role in NF-κB and cytokine transduction.[48] The differences of these genes in different CuPS groups suggest the mechanism basis for the influence of cuproptosis on immune microenvironment. Combined with the difference of WNT pathway in patients with different Cu-RG classes, WNT/β-catenin may be an important pathway for cuproptosis to affect tumor immune microenvironment.

In the overview of mutation characteristics, we observed that the higher mutation rate of ARID1A in the low-CuPS subgroup, which had a high TMB level. ARID1A is a key gene for maintaining genomic stability, and mutation of ARID1A is usually associated with higher TMB level. Meanwhile, the ARID1A can regulate the lipid metabolism and tricarboxylic acid cycle in the metabolic process.[49,50] In addition, in ARID1A-deficient cancer cells, GCLC Inhibition can significantly reduce intracellular GSH, resulting in excessive reactive oxygen species triggering apoptosis.[51] Given that GSH is an intracellular copper chelator,[52] the ARID1A pathway may be a viable target for inducing cell copper death.

In terms of immune characteristics, CuPS was significantly negatively correlated with TMB level, and patients with low CuPS have higher MSI-H ratio and PD-L1 levels, suggesting that patients with low CuPS levels are more likely to benefit from ICIs treatment. To further verify this phenomenon, we transfer the CuPS method to patients in the IMVigor-210 cohort[35] and verified that patients with low CuPS had better response and prognosis in ICIs treatment, suggesting that CuPS may be a predictive marker of sensitivity in ICIs treatment.

In summary, we analyzed the genomic characteristics of cuproptosis-related genes in gastric cancer, constructed cuproptosis-related gene scores (Cg-score), and analyzed the association between cuproptosis level and tumor genomic characteristics, including the immune microenvironment. Finally, we constructed a 3-gene (AHCYL2, ANKRD6, and PDGFRB) cuproptosis-related prognosis signature (CuPS),

https://doi.org/10.1021/acsomega.2c07052
ACS Omega 2023, 8, 10851−10862

which can be used to evaluate the microenvironment of gastric cancer. The CuPS might have the potential value for predicting prognosis and immunotherapy sensitivity in gastric cancer patients.

■ ASSOCIATED CONTENT

Data Availability Statement

All data in this study could be obtained from the UCSC Web site https://xena.ucsc.edu/, TCGA database https://portal.gdc.cancer.gov/ and GEO database https://www.ncbi.nlm.nih.gov/geo/.

Supporting Information

The Supporting Information is available free of charge at https://pubs.acs.org/doi/10.1021/acsomega.2c07052.

Figure S1. Analysis flowchart of this study; Figure S2. Identification of cuproptosis-mediated patterns by NMF clustering; Figure S3. Identification of cuproptosis-related gene subtypse by NMF clustering; Figure S4. Screening of prognosis-related Cu-RGs via Lasso and Cox regression; Figure S5. K−M analysis for OS of AHCYL2, ANKRD6 and FDGFRB in 4 different GC cohorts; Figure S6. Survival meta-analysis of 3 CuPS feature genes in 6 independent GC cohorts; Figure S7. Expression validation of the 3 hub genes by RT-qPCR and immunohistochemistry; and Figure S8. CuPS and patient survival status in GSE84337 and TCGA-STAD cohorts. (PDF)

■ AUTHOR INFORMATION

Corresponding Authors

Hong-Mei Zhang − *Department of Clinical Oncology, Xijing Hospital, Fourth Military Medical University, Xi'an, Shaanxi 710032, P. R. China*; Email: zhm@fmmu.edu.cn

Jianyong Zheng − *Division of Digestive Surgery, Xijing Hospital of Digestive Diseases, Fourth Military Medical University, Xi'an, Shaanxi 710032, P. R. China*; Email: zhjy68@163.com

Authors

Xiang-Xu Wang − *Department of Clinical Oncology, Xijing Hospital, Fourth Military Medical University, Xi'an, Shaanxi 710032, P. R. China*; orcid.org/0000-0002-1658-953X

Shi-Zhou Deng − *Department of Clinical Oncology, Xijing Hospital, Fourth Military Medical University, Xi'an, Shaanxi 710032, P. R. China*

Li-Hong Wu − *Xijing 986 Hospital Department, Fourth Military Medical University, Xi'an, Shaanxi 710032, P. R. China*

Qing-Qing Liu − *Department of Clinical Oncology, Xijing Hospital, Fourth Military Medical University, Xi'an, Shaanxi 710032, P. R. China*

Gaozan Zheng − *Division of Digestive Surgery, Xijing Hospital of Digestive Diseases, Fourth Military Medical University, Xi'an, Shaanxi 710032, P. R. China*

Kunli Du − *Division of Digestive Surgery, Xijing Hospital of Digestive Diseases, Fourth Military Medical University, Xi'an, Shaanxi 710032, P. R. China*

Qiong-Yi Dou − *Department of Clinical Oncology, Xijing Hospital, Fourth Military Medical University, Xi'an, Shaanxi 710032, P. R. China*

Complete contact information is available at: https://pubs.acs.org/10.1021/acsomega.2c07052

Author Contributions

[‖]These authors contributed equally to this work. Conceptualization, X.-X.W., H.-M.Z. and J.Z.; Data curation, X.-X.W., L.-H.W. and S.-Z.D.; Formal analysis, X.-X.W.; Investigation, J.Z., G.Z., K.D. and Q.-Y.D.; Methodology, X.-X.W. and S.-Z.D.; Project administration, H.-M.Z.; Software, X.-X.W.; Supervision, W.P.; Visualization, L.-H.W., Q.-Y.D., Q.-Q.L. and H.-M.Z.; Writing−original draft, X.-X.W. and L.-H.W.; Writing−review and editing, X.-X.W. and H.-M.Z. All authors have read and agreed to the published version of the manuscript.

Funding

This study was supported by the Natural Science Basic Research Program of Shaanxi (No. 2021JZ-35) and National Natural Science Foundation of China (82072655).

Notes

The authors declare no competing financial interest.

■ REFERENCES

(1) Sung, H.; Ferlay, J.; Siegel, R. L.; Laversanne, M.; Soerjomataram, I.; Jemal, A.; Bray, F. Global cancer statistics 2020: globocan estimates of incidence and mortality worldwide for 36 cancers in 185 countries. *Ca-Cancer J. Clin.* **2021**, *71* (3), 209−249.

(2) Smyth, E. C.; Nilsson, M.; Grabsch, H. I.; van Grieken, N. C.; Lordick, F. Gastric cancer. *Lancet* **2020**, *396* (10251), 635−648.

(3) Roviello, G.; Catalano, M.; Iannone, L. F.; Marano, L.; Brugia, M.; Rossi, G.; Aprile, G.; Antonuzzo, L. Current status and future perspectives in her2 positive advanced gastric cancer. *Clin. Transl. Oncol.* **2022**, *24* (6), 981−996.

(4) Nakamura, Y.; Kawazoe, A.; Lordick, F.; Janjigian, Y. Y.; Shitara, K. Biomarker-targeted therapies for advanced-stage gastric and gastro-oesophageal junction cancers: an emerging paradigm. *Nat. Rev. Clin. Oncol.* **2021**, *18* (8), 473−487.

(5) Takei, S.; Kawazoe, A.; Shitara, K. The new era of immunotherapy in gastric cancer. *Cancers* **2022**, *14* (4), 1054.

(6) Kim, B. E.; Nevitt, T.; Thiele, D. J. Mechanisms for copper acquisition, distribution and regulation. *Nat. Chem. Biol.* **2008**, *4* (3), 176−185.

(7) Ge, E. J.; Bush, A. I.; Casini, A.; Cobine, P. A.; Cross, J. R.; Denicola, G. M.; Dou, Q. P.; Franz, K. J.; Gohil, V. M.; Gupta, S.; et al. Connecting copper and cancer: from transition metal signalling to metalloplasia. *Nat. Rev. Cancer* **2022**, *22* (2), 102−113.

(8) Rae, T. D.; Schmidt, P. J.; Pufahl, R. A.; Culotta, V. C.; O'Halloran, T. V. Undetectable intracellular free copper: the requirement of a copper chaperone for superoxide dismutase. *Science* **1999**, *284* (5415), 805−808.

(9) Mohamed, M.; Johnston, A.; Cross, A. M.; Sharma, A. Reversible pancytopenia caused by severe copper deficiency in a patient with wilson disease. *Med. J. Aust.* **2018**, *209* (1), 11−12.

(10) Chen, J.; Jiang, Y.; Shi, H.; Peng, Y.; Fan, X.; Li, C. The molecular mechanisms of copper metabolism and its roles in human diseases. *Pflugers Arch.* **2020**, *472* (10), 1415−1429.

(11) Aggarwal, A.; Bhatt, M. Wilson disease. *Curr. Opin. Neurol.* **2020**, *33* (4), 534−542.

(12) Ramchandani, D.; Berisa, M.; Tavarez, D. A.; Li, Z.; Miele, M.; Bai, Y.; Lee, S. B.; Ban, Y.; Dephoure, N.; Hendrickson, R. C.; et al. Copper depletion modulates mitochondrial oxidative phosphorylation to impair triple negative breast cancer metastasis. *Nat. Commun.* **2021**, *12* (1), 7311.

(13) Guo, J.; Cheng, J.; Zheng, N.; Zhang, X.; Dai, X.; Zhang, L.; Hu, C.; Wu, X.; Jiang, Q.; Wu, D.; Okada, H.; Pandolfi, P. P.; Wei, W.; et al. Copper promotes tumorigenesis by activating the pdk1-akt oncogenic pathway in a copper transporter 1 dependent manner. *Adv. Sci.* **2021**, *8* (18), 2004303.

(14) Shanbhag, V.; Jasmer-Mcdonald, K.; Zhu, S.; Martin, A. L.; Gudekar, N.; Khan, A.; Ladomersky, E.; Singh, K.; Weisman, G. A.; Petris, M. J. Atp7a delivers copper to the lysyl oxidase family of

enzymes and promotes tumorigenesis and metastasis. *Proc. Natl. Acad. Sci. U. S. A.* **2019**, *116* (14), 6836−6841.
(15) Jin, J.; Ma, M.; Shi, S.; Wang, J.; Xiao, P.; Yu, H. F.; Zhang, C.; Guo, Q.; Yu, Z.; Lou, Z.; et al. Copper enhances genotoxic drug resistance via atox1 activated dna damage repair. *Cancer Lett.* **2022**, *536*, 215651.
(16) Zhang, T.; Kephart, J.; Bronson, E.; Anand, M.; Daly, C.; Spasojevic, I.; Bakthavatsalam, S.; Franz, K.; Berg, H.; Karachaliou, G. S.; et al. Prospective clinical trial of disulfiram plus copper in men with metastatic castration-resistant prostate cancer. *Prostate* **2022**, *82* (7), 858−866.
(17) Yang, M.; Wu, X.; Hu, J.; Wang, Y.; Wang, Y.; Zhang, L.; Huang, W.; Wang, X.; Li, N.; Liao, L.; et al. Commd10 inhibits hif1alpha/cp loop to enhance ferroptosis and radiosensitivity by disrupting cu-fe balance in hepatocellular carcinoma. *J. Hepatol.* **2022**, *76* (5), 1138−1150.
(18) Tsvetkov, P.; Coy, S.; Petrova, B.; Dreishpoon, M.; Verma, A.; Abdusamad, M.; Rossen, J.; Joesch-Cohen, L.; Humeidi, R.; Spangler, R. D.; et al. Copper induces cell death by targeting lipoylated tca cycle proteins. *Science* **2022**, *375* (6586), 1254−1261.
(19) Rahman, M.; Jackson, L. K.; Johnson, W. E.; Li, D. Y.; Bild, A. H.; Piccolo, S. R. Alternative preprocessing of rna-sequencing data in the cancer genome atlas leads to improved analysis results. *Bioinformatics* **2015**, *31* (22), 3666−3672.
(20) Chong, W.; Shang, L.; Liu, J.; Fang, Z.; Du, F.; Wu, H.; Liu, Y.; Wang, Z.; Chen, Y.; Jia, S.; et al. M(6)a regulator-based methylation modification patterns characterized by distinct tumor microenvironment immune profiles in colon cancer. *Theranostics* **2021**, *11* (5), 2201−2217.
(21) Cai, Y.; Gu, H.; Kenney, T. Learning microbial community structures with supervised and unsupervised non-negative matrix factorization. *Microbiome* **2017**, *5* (1), 110.
(22) Hanzelmann, S.; Castelo, R.; Guinney, J. Gsva: gene set variation analysis for microarray and rna-seq data. *Bmc Bioinformatics* **2013**, *14*, 7.
(23) Liberzon, A.; Birger, C.; Thorvaldsdottir, H.; Ghandi, M.; Mesirov, J. P.; Tamayo, P. The molecular signatures database (msigdb) hallmark gene set collection. *Cell Syst.* **2015**, *1* (6), 417−425.
(24) Yu, G.; Wang, L. G.; Han, Y.; He, Q. Y. Clusterprofiler: an r package for comparing biological themes among gene clusters. *Omics* **2012**, *16* (5), 284−287.
(25) Newman, A. M.; Liu, C. L.; Green, M. R.; Gentles, A. J.; Feng, W.; Xu, Y.; Hoang, C. D.; Diehn, M.; Alizadeh, A. A. Robust enumeration of cell subsets from tissue expression profiles. *Nat. Methods* **2015**, *12* (5), 453−457.
(26) Becht, E.; Giraldo, N. A.; Lacroix, L.; Buttard, B.; Elarouci, N.; Petitprez, F.; Selves, J.; Laurent-Puig, P.; Sautes-Fridman, C.; Fridman, W. H.; et al. Estimating the population abundance of tissue-infiltrating immune and stromal cell populations using gene expression. *Genome Biol.* **2016**, *17* (1), 218.
(27) Tirier, S. M.; Mallm, J. P.; Steiger, S.; Poos, A. M.; Awwad, M.; Giesen, N.; Casiraghi, N.; Susak, H.; Bauer, K.; Baumann, A.; et al. Subclone-specific microenvironmental impact and drug response in refractory multiple myeloma revealed by single-cell transcriptomics. *Nat. Commun.* **2021**, *12* (1), 6960.
(28) Zeng, D.; Li, M.; Zhou, R.; Zhang, J.; Sun, H.; Shi, M.; Bin, J.; Liao, Y.; Rao, J.; Liao, W. Tumor microenvironment characterization in gastric cancer identifies prognostic and immunotherapeutically relevant gene signatures. *Cancer Immunol. Res.* **2019**, *7* (5), 737−750.
(29) Zhang, B.; Wu, Q.; Li, B.; Wang, D.; Wang, L.; Zhou, Y. L. M(6)a regulator-mediated methylation modification patterns and tumor microenvironment infiltration characterization in gastric cancer. *Mol. Cancer* **2020**, *19* (1), 53.
(30) Feng, D.; Xiong, Q.; Zhang, F.; Shi, X.; Xu, H.; Wei, W.; Ai, J.; Yang, L. Identification of a novel nomogram to predict progression based on the circadian clock and insights into the tumor immune microenvironment in prostate cancer. *Front. Immunol.* **2022**, *13*, 777724.
(31) Schwarzer, G. An r package for meta-analysis. *R News* **2007**, No. 7, 40−45.
(32) Qin, Y.; Luan, J.; Zhou, X.; Li, Y. Pd-l1 expression in anogenital and oropharyngeal squamous cell carcinomas associated with different clinicopathological features, hpv status and prognosis: a meta-analysis. *Biosci. Rep.* **2021**, *41*(3), DOI: DOI: 10.1042/BSR20203669.
(33) Geeleher, P.; Cox, N.; Huang, R. S. Prrophetic: an r package for prediction of clinical chemotherapeutic response from tumor gene expression levels. *PLoS One* **2014**, *9* (9), e107468.
(34) Mariathasan, S.; Turley, S. J.; Nickles, D.; Castiglioni, A.; Yuen, K.; Wang, Y.; Kadel, E. I.; Koeppen, H.; Astarita, J. L.; Cubas, R.; et al. Tgfbeta attenuates tumour response to pd-l1 blockade by contributing to exclusion of t cells. *Nature* **2018**, *554* (7693), 544−548.
(35) Balar, A. V.; Galsky, M. D.; Rosenberg, J. E.; Powles, T.; Petrylak, D. P.; Bellmunt, J.; Loriot, Y.; Necchi, A.; Hoffman-Censits, J.; Perez-Gracia, J. L.; et al. Atezolizumab as first-line treatment in cisplatin-ineligible patients with locally advanced and metastatic urothelial carcinoma: a single-arm, multicentre, phase 2 trial. *Lancet* **2017**, *389* (10064), 67−76.
(36) Feng, Y.; Zeng, J. W.; Ma, Q.; Zhang, S.; Tang, J.; Feng, J. F. Serum copper and zinc levels in breast cancer: a meta-analysis. *J. Trace Elem. Med. Biol.* **2020**, *62*, 126629.
(37) Wang, J.; Luo, C.; Shan, C.; You, Q.; Lu, J.; Elf, S.; Zhou, Y.; Wen, Y.; Vinkenborg, J. L.; Fan, J.; et al. Inhibition of human copper trafficking by a small molecule significantly attenuates cancer cell proliferation. *Nat. Chem.* **2015**, *7* (12), 968−979.
(38) Wu, Z.; Zhang, W.; Kang, Y. J. Copper affects the binding of hif-1alpha to the critical motifs of its target genes. *Metallomics* **2019**, *11* (2), 429−438.
(39) Zimna, A.; Kurpisz, M. Hypoxia-inducible factor-1 in physiological and pathophysiological angiogenesis: applications and therapies. *Biomed Res. Int.* **2015**, *2015*, 549412.
(40) Cobine, P. A.; Brady, D. C. Cuproptosis: cellular and molecular mechanisms underlying copper-induced cell death. *Mol. Cell* **2022**, *82* (10), 1786−1787.
(41) Wu, Z. H.; Tang, Y.; Yu, H.; Li, H. D. The role of ferroptosis in breast cancer patients: a comprehensive analysis. *Cell Death Discovery* **2021**, *7* (1), 93.
(42) Jorgovanovic, D.; Song, M.; Wang, L.; Zhang, Y. Roles of ifn-gamma in tumor progression and regression: a review. *Biomark. Res.* **2020**, *8*, 49.
(43) Katoh, M. Canonical and non-canonical wnt signaling in cancer stem cells and their niches: cellular heterogeneity, omics reprogramming, targeted therapy and tumor plasticity (review). *Int. J. Oncol.* **2017**, *51* (5), 1357−1369.
(44) Grasso, C. S.; Tsoi, J.; Onyshchenko, M.; Abril-Rodriguez, G.; Ross-Macdonald, P.; Wind-Rotolo, M.; Champhekar, A.; Medina, E.; Torrejon, D. Y.; Shin, D. S.; et al. Conserved interferon-gamma signaling drives clinical response to immune checkpoint blockade therapy in melanoma. *Cancer Cell* **2020**, *38* (4), 500−515.
(45) Huang, W.; Li, N.; Zhang, Y.; Wang, X.; Yin, M.; Lei, Q. Y. Ahcyl1 senses sah to inhibit autophagy through interaction with pik3c3 in an mtorc1-independent manner. *Autophagy* **2022**, *18* (2), 309−319.
(46) Yamaguchi, S.; Ishikawa, T. Ahcyl2 (long-irbit) as a potential regulator of the electrogenic na(+)-hco3(−) cotransporter nbce1-b. *Febs Lett.* **2014**, *588* (5), 672−677.
(47) Katoh, M. Wnt/pcp signaling pathway and human cancer (review). *Oncol. Rep.* **2005**, *14* (6), 1583−1588.
(48) Kazlauskas, A. Pdgfs and their receptors. *Gene* **2017**, *614*, 1−7.
(49) Qu, Y. L.; Deng, C. H.; Luo, Q.; Shang, X. Y.; Wu, J. X.; Shi, Y.; Wang, L.; Han, Z. G. Arid1a regulates insulin sensitivity and lipid metabolism. *Ebiomedicine* **2019**, *42*, 481−493.
(50) Ogiwara, H.; Takahashi, K.; Sasaki, M.; Kuroda, T.; Yoshida, H.; Watanabe, R.; Maruyama, A.; Makinoshima, H.; Chiwaki, F.; Sasaki, H.; et al. Targeting the vulnerability of glutathione metabolism in arid1a-deficient cancers. *Cancer Cell* **2019**, *35* (2), 177−190.
(51) Ogiwara, H.; Takahashi, K.; Sasaki, M.; Kuroda, T.; Yoshida, H.; Watanabe, R.; Maruyama, A.; Makinoshima, H.; Chiwaki, F.;

Sasaki, H.; et al. Targeting the vulnerability of glutathione metabolism in arid1a-deficient cancers. *Cancer Cell* **2019**, *35* (2), 177−190.
(52) Li, S.; Cao, D.; Meng, X.; Hu, Z.; Li, Z.; Yuan, C.; Zhou, T.; Han, X.; Ma, W. A novel fluorescent sensor for specific recognition of gsh based on the copper complex and its bioimaging in living cells. *Bioorganic Chem.* **2020**, *100*, 103923.

https://doi.org/10.1021/acsomega.2c07052
ACS Omega 2023, 8, 10851−10862